RSC Advances

Preparation and Characterization of Magnetic Nanoparticles and their Impact on Anticancer Drug Binding and Release Processes Moderated Through 1st Tier Dendrimer

Journal:	*RSC Advances*
Manuscript ID	RA-ART-01-2016-002139.R1
Article Type:	Paper
Date Submitted by the Author:	18-Mar-2016
Complete List of Authors:	Pandya, Shivani; Central University of Gujarat, Centre for Nanoscience Singh, Man; Central University of Gujarat, School of Chemical sciences
Subject area & keyword:	Nanotechnology < Chemical biology & medicinal

Journal Name

ARTICLE

Preparation and Characterization of Magnetic Nanoparticles and their Impact on Anticancer Drug Binding and Release Processes Moderated Through 1st Tier Dendrimer

Received 00th January 20xx,
Accepted 00th January 20xx

DOI: 10.1039/x0xx00000x

www.rsc.org/

Shivani R Pandya[a] and Man Singh[ab*]

The Magnetic nanoparticles accumulated dendrimers (MAD) have been prepared by taking 1:1 ratio of MNPs and trimesoyl 1, 3, 5- trimethyl malonate ester (TTDMM) 1st tier dendrimer in ethanolic medium at 100 °C on refluxing for 24 h. Formation of MAD was characterized for their structural, functional and morphological properties by using XRD, VSM, FTIR, SEM–EDX, TEM and DLS techniques. The MNPs shows superparamagnetic character which moderates the structural abilities of TTDMM to bind the silibinin (SB) and methotrexate (MTX) anticancer drugs for their potential use in drug delivery system. In this context, MAD has shown higher silibinin and methotrexate binding activities as comparable to dendrimer only, which are confirmed through FTIR, DLS and SEM-EDX. UV-Vis spectrophotometry study shows 32.65 % and 53.03 % in vitro release of SB and MTX respectively at 10h, in PBS with 10 % DMSO (PD) medium at 37 °C. Furthermore the chemosensitivity testing of MAD was carried out on human lung cancer cell line (A549) using sulforhodamine B (SRB) assay. The test showed that the newly developed drug delivery system for SB and MTX inhibits the growth of A549 human lung cancer cells by 13.9% and 44.3% respectively with 80 µg/ml. The results of our study have provided new insight for developing MAD as a potential carrier for anticancer drug binding with a controlled and sustained release tendency.

1. Introduction

Currently, intensive efforts have been in progress to develop the nanomaterials with broad applications in biomedical and pharmaceuticals to increase the bioavailability of drugs. Research in the area of drug nanocarriers is a century old challenging task for efficient and safer curing of disease which rest on the bioavailability and drugs efficiency. And thus, there is a significant thrust prevalent in terms of the accuracy and effectiveness of the corresponding drug systems that sometimes cause little over-dosage of delivering drugs, damaging the normal cells and leading to the side effects [1]. In such situations, the MNPs are one of the most promising and potential candidates in the domain of biomedical and pharmaceutical applications. Presently, several exciting developments and methodologies for the synthesis and characterization of MNPs are being driven through their distinct and multifold applications, via their incorporation in the form of structural nanomaterials [2]. The applications of MNPs in various domains including drug delivery systems, catalysis, medical applications, for instance, magnetic resonance imaging (MRI), medical diagnostics and cancer therapy, magneto-optics devices, sensors, microelectronic circuiting, coatings, building blocks for nanotechnology based networks and many others have drawn the attention of the scientist [3-6]. However, up to some extent the surface modified MNPs using various bioactive molecules have fastened and improve the bioavailability of the drug at targeted sites [7]. Due to the above-mentioned properties the MNPs have been first time introduced as a potential drug carrier for clinical applications in the 1970s. During the year, 1978 both, Senyei et al and Widdeer et al have proposed the MNPs application for antitumor drug delivery system [8, 9]. In 1996, Lubbe et al reported about the phase-I clinical test of MNPs as a carrier for targeted drug delivery of 4'- Epidoxorubicin by making its complex via electrostatic interaction between the phosphate groups on the surface of the MNPs and amino sugars present in drug [10, 11]. Also, the Koda et al reported the doxorubicin hydrochloride drug delivery by using MNPs as a carrier. They have prepared the MNPs-Drug and targeted to the tumour site using an external magnetic field and the localization of particles scanned with MRI [12, 13]. Up to now many research groups have reported the MNPs synthesis and their functionalization by using different coating agents, further they enabled them to be used as cancer drug carriers with controlled degradation [14-19]. Recently, MNPs were functionalized with various biomolecules like DNA, Peptides, Lipids, Antibodies and Primers to enhance the specificity and solubility and to reduce the side effects [20, 21].

Like MNPs as inorganic oxide nanoparticles, dendrimers are well-defined organic nanoparticles having a hyperbranched structure with the size distribution within 1-15 nm with versatile surface functionalization. The above-mentioned properties have facilitated bioavailability and protection of

[a] Centre for Nanosciences, Central University of Gujarat, Gandhinagar, India.
[b] School of Chemical Sciences, Central University of Gujarat, Gandhinagar-382030, India.
E-mail: shivpan02@gmail.com, *mansingh50@hotmail.com

Electronic Supplementary Information (ESI) available: [Supplementary data sheet is attached]. See DOI: 10.1039/x0xx00000x

drug molecules against premature degradation through the cell barrier [22, 23]. Dendrimers can use as a drug vehicle either by encapsulating drugs within their dendritic structural framework or by interacting with drugs at their terminal functional group via electrostatic or weak Vader Waals forces [24-26]. Encasing such advantages of MNPs and dendrimers together the novel structure could be generated with high surface activities for targeted and sustained drug release. For instance, Pan Bifeng et al. reported MNPs coated with PAMAM dendrimer enhance the efficiency of gene delivery system with potential application in cancer therapy and molecular imaging diagnosis [27]. Currently, Chang et al., Rouhollah et al. and Khodadust et al. individually observed an increase in the loading capacity of Doxorubicin in PAMAM coated MNPs for targeted drug delivery to avoid serious side effects [28-30]. Also, several studies have been focused for protein immobilization using dendrimer modified MNPs supported the use in biological and medical sciences [31]. Naturalium observed the application of Metallo-dendrimers in catalysis, nanoparticle stabilization, biomedical and tissue engineering applications [32]. The formulation of highly efficient drug binding materials have been a century old challenging task for better and safer curing of the disease on account of an efficient drug delivery. In our earlier work, the synthesis and characterization of TTDMM and their application as a potential carrier for SB drug delivery systems had been reported [33]. The dendrimer coated MNPs have been found befitting entities, although the uneven distribution of their electrostatic charges could be a slight restriction which could damage a drug structure and efficiency due to a possibility of chemical reaction. In our previous work, we reported that 1:1 ratio of MNPs with TTDMM shows maximum interaction in DMSO [34].

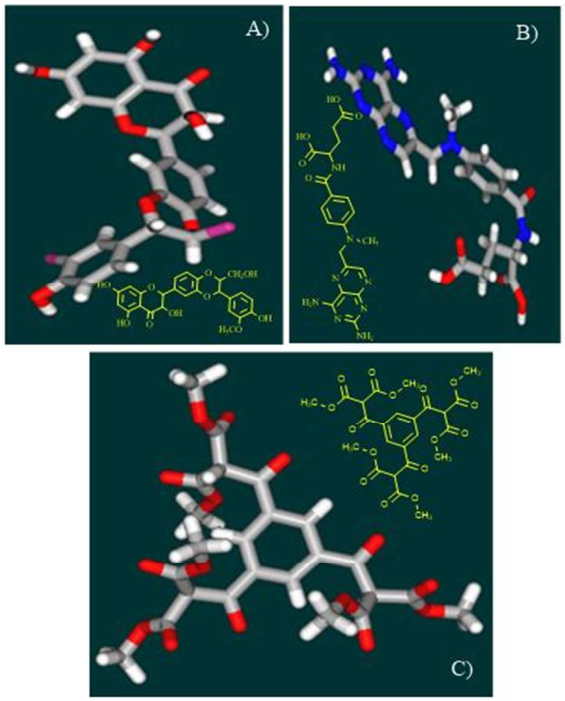

Fig.1. Molecular structures of A) Silibinin, B) Methotrexate and C) TTDMM 1st tier dendrimer

Hence, in this work, the MAD has been prepared, which could be act as an efficient drug carrier system. The MAD may be having a tendency to aggregate in an aqueous medium with hydrophobic nature, due to their high specific surface area and surface free energy [34].

The SB is a very important flavanone with an immunomodulatory effect such as anticancer, chemopreventive and antioxidant activities [35, 36]. The MTX is an anticancer drug extensively used as in chemotherapeutic agent against effective in treating breast, lung, bone and cervical cancer, as well as leukaemia (Fig. 1) [37]. The SB and MTX normally administrated through oral route in an encapsulated form due to their poor water solubility and higher dosages causing side effects [38-40]. The SB and MTX require novel formulations for enhancing their bioavailability and subsequently improve the bioactivity. In this work, we have focused on MAD to enhance its binding and control releasing activities of SB and MTX. This intensive study could be progressed to develop MNPs for biomedical use as agents for targeted specific drug delivery systems.

2. Material and Methods

2.1 Materials

Iron (II) sulfate heptahydrate ($FeSO_4.7H_2O$), Ferric chloride ($FeCl_3$), silibinin (SB), methotrexate (MTX), acetone and phosphate buffer saline (PBS) tablets were all purchased from Sigma-Aldrich, ethanol was purchased from Scvuksmandli Ltd. Sodium hydroxide (NaOH) and Dimethyl sulfoxide (DMSO) was purchased from Rankem India. Corning sterile syringe filter 0.20 µm was purchased from Germany.

2.2 Synthesis of MNPs

Synthesis of MNP was carried out as we reported a method using co-precipitation of 0.2 M $FeCl_3$ and 0.1M $FeSO_4.7H_2O$ in 2:1 ratio followed by the addition of aqueous 8M NaOH till pH increase to 12-13 at 90 °C and continuously stirred for 2 h at 1000 rpm [34]. The obtained MNPs were washed with warmed Milli- Q water for 3-4 times, followed by washing with ethanol. The MNPs were separated by magnetic decantation and vacuum dried overnight at 67 °C. The MNPs were stored in Borosil sample tube at 37 °C.

2.3 Preparation of MAD

The MAD was carried out using dendrimers and MNPs in 1:3 ratios respectively. The MNPs were dispersed in ethanol and refluxed at 100 °C for 2 h. After 2 h, the TTDMM was added to the ethanol-MNPs dispersion. The TTDMM-MNPs in ethanol refluxed at 100 °C for 24 h followed by ethanol evaporation from the mixture by using a rotary evaporator at 78.3 °C. On evaporation of ethanol, the brown colored product was obtained that showed magnetic properties.

2.4 Drug-MAD complex preparation

The SB-MAD and MTX-MAD binding was prepared by mixing SB and MTX with MAD separately in (1:1, mol/mol) in 30 ml acetone at constant stirring with 600 rpm for 36 h at RT. After

36 h, the acetone was evaporated at 56 °C in vacuum using Rotavapor (R-210, Buchi, Switzerland).

2.5 Characterization

2.5.1 High-resolution transmission electron microscopy

High-resolution transmission electron microscopy images were taken using JEOL JEM 2100 LaB6 (JEOL USA, Inc.) on applying an acceleration voltage of 200 kV in imaging mode, which results in a wavelength of 2.5 pm. For observation by TEM, an aliquot of a sonicated suspension of MNPs and MAD powdered samples in toluene/acetone was added dropwise onto a 200 mesh copper grid.

2.5.2 X-Ray Diffraction

A RICH-SEIFERT diffractometer (PTS 3000, Germany) was used for determining the interplanar distances (dhkl) and crystalline phase present in the sample using θ/2θ measurements. 2 g of powder sample was mounted on the holder for further analysis. The Cu Kα radiation at λ = 1.54 A° used as the X-ray source, and operated with 40 kV voltage and 30 mA cathodic current. The spectrum was recorded from 5 to 80° at 0.01 degrees/scan rate. The Bragg's law (1) and the lattice parameter (2) equations were used to determine the interplanar spacing.

$$d_{hkl} = \frac{\lambda}{2\sin\theta} \quad (1)$$

$$d_{hkl} = \frac{a}{\sqrt{h^2 + k^2 + l^2}} \quad (2)$$

Where, θ is the half diffraction angle and h, k, l as the Miller indices of the diffraction plane.
The crystallite size was calculated by the Debye–Scherrer equation (3) [41],

$$L_{hkl} = \frac{0.9\,\lambda}{\beta.\cos\theta} \quad (3)$$

Where, β is a full-width at half-maximum (FWHM) value of XRD diffraction lines.

2.5.3 Magnetization

Magnetization was measured using vibrating sample magnetometer (PPMS-VSM 14T, Quantum Design) using 100 Oe/sec magnetic fields in driving mode using Nb_3Sn magnet between +40 to -40 kOe longitude at 300 K with the sensitivity of 10^{-5} emu and 0.5 % accuracy. Sample preparation was carried out by filling sample in the cylindrical sample vial of diameter 3 mm X 10 mm and closely packed vials were mounted on the brass half tube sample holder having fused quartz paddles for magnetization measurements.

2.5.4 Fourier transforms infrared spectroscopy

The chemical composition and complex formation of the samples was determined using a Perkin-Elmer 65 series FTIR spectrophotometer. To prepare a sample for FTIR analysis, 1.5 to 2.0 mg was mixed with 200 mg KBr for making pellets which were kept in the KBr press machine (model Mp-15) by applying 5 kg/cm_2 for 2-3 min. After a background scan, the sample was analyzed at 400-4000 cm^{-1}.

2.5.5 Mean diameter and polydispersity index

A mean diameter (MD) and polydispersity index (PDI) were determined by Dynamic Light Scattering (DLS) device (Microtrac Zetatrac Metrohome U2771) operated at 180° backscattering mode with two laser source (λ =780 nm) at 25 °C. The particles were dispersed in 40% aq. tween 60. The experiments have been done in triplets.

2.5.6 Scanning Electron Microscopy

The surface morphology of MNPs, dendrimers, and the complexes were studied with SEM-EDX (Carl Zeiss, and EVO-18) operated at 20 kV. The solid sample was coated using a thin layer of palladium and gold in 80:20 ratio by sputtering at 5 µA current up to 60 Sec for making conducting surface before recording SEM micrographs. The sputtering has enhanced the resolution of the micrographs.

2.5.7 Drug entrapment efficiency

The total drug in the prepared nanoparticles was determined by dissolving Drug-MNPs in 70% w/v ethanol solution. The solution was then filtered through 0.20 µm (Corning, Germany) filters and assayed for drug content by UV-Vis spectrophotometry. The percentage of entrapment efficiency was determined by the formula,

$$\%\,Entrapment\ efficiency = \frac{A_{(total\ drug)} - A_{(free\ drug)}}{A_{(total\ drug)}}\ X\ 100 \quad (4)$$

Where, A (total drug) is the optical density (OD) of the drug loaded nanoparticles and A (free drug) is the OD of filtrate containing the free drug.

2.6 *In vitro* drug release study

The 25, 50, 75, 100 and 125 µM SB and MTX each were dissolved in PD individually for the calibration curve. The 10 mg complex was separately dissolved in 100 ml PD (pH 7.4) and stirred continuously at 100 rpm at 37 °C. The 3 ml sample was withdrawn through a sampling syringe attached to a sterile syringe filter, 0.20 µm at predetermined time intervals (0-10 h). The collected samples were then analyzed for SB content by measuring absorbance at 245, 285 and 330 nm and for MTX 260, 305 and 375 nm with UV/Vis spectrophotometer (Spectro 2060 plus model) over 200-600 nm using 1 cm path length quartz cuvette. The SB and MTX concentration and % release were determined by Equation (5) and (6) [42-45].

$$A = \varepsilon \times l \times c \quad (5)$$

The A is an absorbance, ε molar absorptivity and *l* cell path length (cm). The c is SB and MTX compositions with 125 µM/L in 100 ml PD and A is 2.187 and 1.812 respectively, and *l* is 1 cm, putting these

values in equation 1, the ε = 0.3645 and 0.3190 m^2/mmol is found at λmax $_{(SB)}$ 330 nm and λmax $_{(MTX)}$ 260 nm respectively.

$$\% \, Drug \, release = \frac{Drug \, released}{Amount \, of \, drug \, in \, substrat} \; X \; 100 \qquad (6)$$

In vitro release experiments were performed in triplicate (n = 3) for each of drug-MAD complexes in an identical manner.

2.7 SRB assay

The chemosensitivity testing of MNP, MAD, SB-MAD, and MTX-MAD were carried using a sulforhodamine B assay on human lungs cancer cell line (A549). The principle of SRB assay is based on the cell proliferation as SRB (an anionic dye) is bound to proteins electrostatically, which were synthesized during proliferation of the cell. The excess amount of unbound dye can be washed out with 1% acetic acid. The air-dried compound was solubilized with 150 µl 10 mmol/l unbuffered Tris base. The optical density was determined at 540 or 510 nm.

3. RESULTS AND DISCUSSION

3.1 HR-TEM

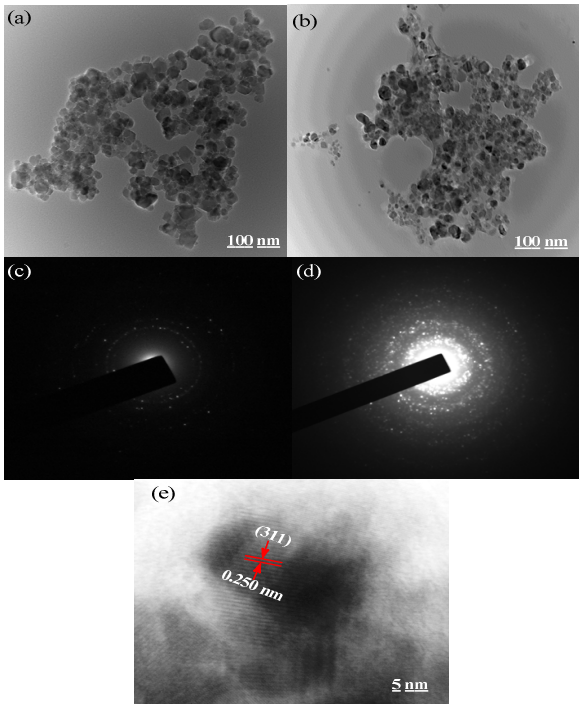

Fig.2. The TEM image of (a) MNPs and (b) MAD, SAED pattern of (c) MNPs and (d) MAD, image (e) shows interplanar spaces of MNPs present in MAD at very high magnification

The HR-TEM images of MNPs and MAD shown in Fig. 2 showed spherical shape and mean size is ~17.70 nm with standard deviation (σ) 2.265 nm (Fig. 2a). The Fig. 2c reveals that the selective area electron diffraction ring (SEAD) of MNPs with a dot pattern of ring confirms a highly crystalline nature. In TEM image of MAD, showed a thin layering of dendrimer with accumulation of MNPs are clearly seen (Fig. 2b). However, the SAED shows polycrystalline nature which confirms the formation of MAD with some porosity (Fig. 2c). Mean size of MAD found ~ 16.71 nm with σ = 2.33 nm.

In the TEM images for MAD with higher magnification, it is possible to see the lattice planes of individual particles, which indicates the magnetite particles are monocrystalline. After calculation according to scale, the strip spacing is found 0.252 nm, which equals to standard interplanar crystal spacing [46] of the Fe_3O_4 having (311) planes in face-centered cubic spinal structure. This corresponds to the XRD spectra which show a major peak at 35.5° of (311) plane. The bright field (BF) and dark field (DF) images of MAD do not show the effective difference of organic layering due to masoporous properties of the complex but, arrow mentioned area show some difference on the basis of the dense accumulation of MNPs within the dendrimers (Fig. S1).

3.2 XRD

The XRD analysis of the MNPs and MAD obtained by are given in Fig. 3 depict, significant XRD patterns of MNPs and MAD. A series of characteristic peaks at (220), (311), (400), (511) and (440) depicts high crystallinity of MNPs, the MAD shows that the same crystal planes as of MNPs with some extra peaks between the 2θ values of 20° to 30° for dendrimers. It is observed that a new lattice plane has been generated at 32°, that indicates the formation of functional interface (FI) between –C=O of TTDMM and octahedral-tetrahedral planes of MNPs. Probably this FI is the result of delocalized electron cloud of TTDMM which might reorient lattice plane of MNPs. These geometrical changes are supported by a morphological change in SEM micrograph (Fig. 7a-7c). The major peak at 35.5° is corresponding to the (311) plane with higher intensity confirmed the magnetite phase of MNP. Other peaks at 30.04° (220), 46.7° (400), 57.04° (511) and 62.2° (440) are less characteristic due to the small crystal size of magnetite. The pure MNPs patterns match the standard XRD data of bulk Magnetite (JPCDS file No. 00-019-629). However, magnetite and maghemite crystallizes in a cubic spinal structure with the distinction that maghemite has 21/3 vacancies confined to octahedral geometry. The d_{hkl} value at peak (311) is 0.2526 nm which is the interplanar spacing between those planes calculated using Bragg's law (1). Using this value the equation (2) gives the lattice parameter a =0.8377 nm. It is very close to the value for magnetite ($a_{magnetite}$ = 0.8396), and away from the value found for maghemite ($a_{maghemite}$ = 0.8347) indicate that the coprecipitation using NaOH without providing inert gas is preferential for the formation of Fe_3O_4 NPs.

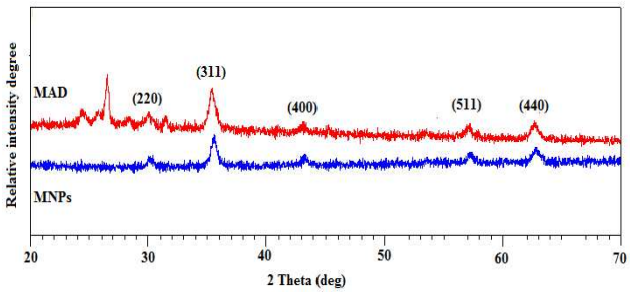

Fig. 3. XRD spectra of (a) MNPs and (b) MAD

By using the FWHM value of the (311) peak crystalline size can be calculated using Debye-Scherrer equation (3) and found as d_{MNPs} = 18 nm and d_{MAD} =16 nm for MNPs and MAD respectively. This infers that the accumulation of MNP in the void spaces of TTDMM did not change the structural properties and crystal nature of MNPs. Although TTDMM showed the catalytic effect to suppress the columbic forces formed within MNPs results in smaller size.

3.3 Magnetization saturation

Magnetization saturation (Ms) of MNPs and MAD were studied with vibrating sample magnetometer (VSM) at room temperature in applied magnetic field sweeping from -40 to +40 kOe and VSM curve shown in Fig 3. The Ms of pure MNPs was found 64 emu/g, which is relatively low as compared to its bulk value 92 emu/g [47]. This behavior is due to a number of defects present on the surface layers of nanosized fine magnetite particles which could not contribute to the magnetization. The Ms of MAD shows a suppression of the magnetic moment up to 30.13 %, which is 19.28 emu/g (Fig. 4). The loss in magnetization is proportional to the amount /weight of (non-magnetic) dendrimers aggregation. This revealed that the accumulation of MNPs within the void spaces of the dendrimer, weaken the intra molecular columbic forces of MNP, which is responsible for the reduction of particle size confirmed through Scherrer's calculation, this leads to reduction in Ms value.

Sample	Mass (g)	Magnetization (emu/g)
MNPs	0.01749	64.00
MAD	0.01137	19.28

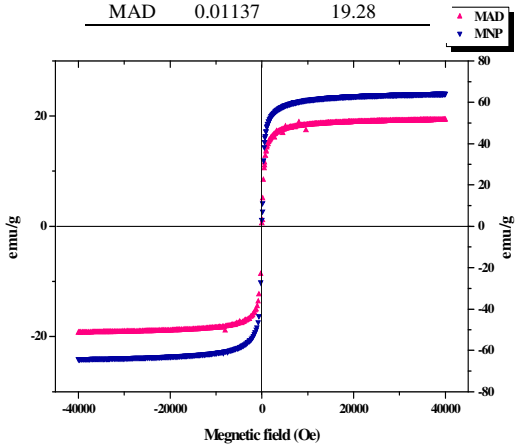

Fig.4. M-H plots of MNP and MAD at 300 K

3.4 FTIR

The FTIR spectroscopy is mainly instrumental technique for understanding the molecular mechanism of the molecules such as identify the functional groups, their binding and interacting activities with foreign molecules. The table 1 shows stretching frequencies of various functional groups present in the compounds. The Figures 5 (a) and S2 show the FTIR spectra of the MAD, MNPs and TTDMM respectively. The peak at 1735 and 1618.4 cm^{-1} due to the carbonyl (>COO) asymmetric stretching frequency of dimethyl malonate ester and aromatic carbonyl (Ar-CO) bonds, respectively, which shifted to lower peak at 1733.3 and 1616.2 cm^{-1} in MAD inferred the binding potential of TTDMM with MNPs monitored via >CO functionality. The reduced intensity of these bands as seen in spectra of MAD revealed that the Fe atom may be bonded to the COO group of a dialkyl malonate ester and the CO of Aromatic ring of TTDMM. The strong absorption band at 559.54 cm^{-1} attributed to the Fe-O stretching vibrational mode of Fe_3O_4 and further, shifted to higher wave numbers at 583.15 cm^{-1} in MAD due the strong electrostatic interaction between >CO and Fe_3O_4.

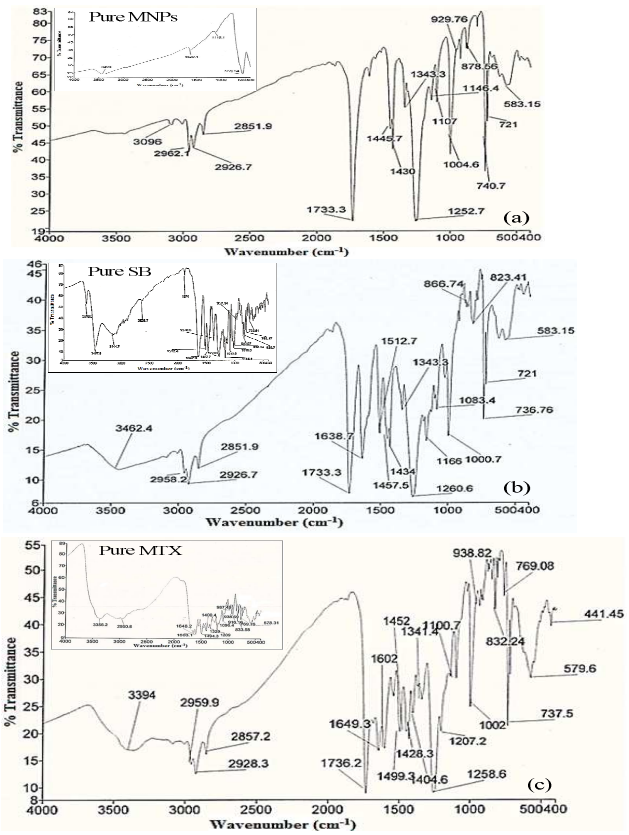

Fig.5. FTIR spectra of, (a) MAD, (b) SB-MAD, (c) MTX-MAD, The inset at left shows spectra of Pure MNPs, SB and MTX respectively

Table. 1. IR stretching frequencies of functional groups.

	Functional groups & Stretching Frequencies (cm^{-1})				
	-COOR	Ar-C=O	>C=O	-OH	Fe-O
TTDMM	1735	1618.4	-	-	-
MNPs	-	-	-	-	559.54
MAD	1733.3	1616.2	-	-	583.15
SB	-	-	1642.9	3457.8	-
MTX	-	-	1648.2	3356.2	-
SB-MAD	1733.3	-	1638.7	3452.4	583.15
MTX-MAD	1736.2	-	1649.3	3394.0	579.6

Probably, the pure TTDMM and TTDMM aggregated MNPs bonding includes a bond between lone pair electrons in -COO and >CO to the Fe with donation of electron density from the metal to carbonyl functionality. This inferred weakening of the C-O bond, which shifted the stretching frequencies at lower peak as seen in the FTIR spectra of MAD. The shifting of stretching frequencies to lower values inferred weakening of the carbonyl bond [48].

Hence, the FTIR results of MAD confirmed the successful aggregation of MNPs with TTDMM. The shifting occurs as a consequence of changes in electron density with respect to the carbonyl group of TTDMM and considerably disrupted due to the formation of the HB for SB binding and release profile which studied through FTIR and UV-Vis spectroscopy as reported elsewhere [33]. Similarly, the binding potential of MAD with SB and MTX has also studied by FTIR. The peak at 1642.9 and 3457.8 cm^{-1} due to the >CO of the ring and –OH bonds in SB, respectively, reflects and shifts to lower wave numbers at 1638.7 and 3452.4 cm^{-1} in SB-MAD revealing the binding of the SB to the MAD through >CO and -OH functionality. Similarly, their intensity shifted from 55 to 12% and 5 to 15% transmission for –OH and >CO respectively, due to the electrostatic interactions that influenced the binding of SB with MAD.

Pure MTX has a typical spectrum pattern which also founds in the MTX-MAD with the shifting of wave numbers, which has confirmed the presence of MTX, loaded in the MAD. The FTIR spectrum of MTX shows the characteristic absorption band as a broad signal at 3356.2, 1648.2 and 2950.8 cm^{-1} corresponds to O–H, >CO and N–H stretching vibrations respectively, shifts to higher wave numbers in MTX-MAD. The peak at 1733.3 cm^{-1} due to the dimethyl malonate ester in MAD which shifted to higher wave numbers at 1736.2 cm^{-1} in MTX-MAD inferred the binding nature of MAD to MTX monitored through >COO functionality. The bands corresponding to N-H bending from amide group appear in the 1500-1494.3 cm^{-1} spectral range and partly overlapping with the aromatic –C=C stretching (Figs. 5c). The strong absorption band at 583.16 cm^{-1} can be attributed to the Fe-O stretching vibrational of Fe and similar observation was made in the case of SB-MAD while in case MTX-MAD shifted to lower wave numbers. Shifting of the respective characteristic peaks and the reduced intensity of the observed bands in SB-MAD and MTX-MAD suggests that the SB and MTX anticancer drugs may be bonded to the dimethyl malonate ester arms and Fe_3O_4 of the MAD as well.

From these results, it is evidently depicted that the molecular mechanism of HB and electrostatic interactions between MAD and drugs (SB and MTX) different with a chemical structure along with a structured activity of MAD. Thereby, the MNPs accumulated dendrimer's structure could be attributed to their involvement in interactions with SB and MTX for encapsulation. The MAD initiates higher activities of the drug binding, due to the aggregation of MNPs, when they enter within the networks of TTDMM.

3.5 Mean diameter and polydispersity index

The MD and PDI results have suggested about the aggregation behavior of MNPs, MAD, SB, MTX, SB-MAD, and MTX-MAD (Figs. 6a, 6b). Their size distribution with 40% tween 60 is seen in figure S3. Since, tween 60 (C=16) has adequate number of –OH groups in polysorbate head and alkyl chain of carbon having the desired hydrophilic-hydrophobic components for robust Brownian motion it has been used as a dispersion medium. The MD values were found 1.13, 12.47, 10.19 and 10.49 nm for SB, MTX, MNPs and MAD respectively (Fig. 6a). Since the Fe_3O_4 MNPs are used for the accumulated with TTDMM. When the MNPs accumulated with the TTDMM shows the slightly higher value of the modified MAD by 0.30 nm as compared to MNPs. Also, these changes were proven from their FTIR study with changing different stretching frequency which corresponds to different functional groups of the MAD. The additional MNPs activities in the void spaces of TTDMM having magnetic properties in MAD implies a higher MD as compared to pure MNPs which confirmed in FTIR study. Singh et al. have reported the 12.00 nm MD of TTDMM, but after aggregated with MNPs found 10.49 and it decreased by 1.51 nm in the same dispersion medium for MAD [33].

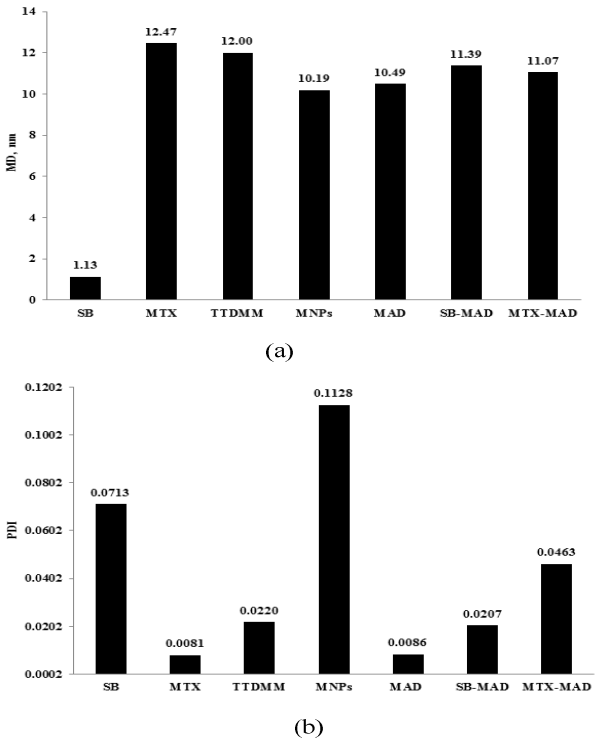

Fig.6. (a) Mean diameter and (b) Poly dispersity index of SB [33], MTX, TTDMM [33], MNPs, MAD, SB-MAD and MTX-MAD

After the aggregation of MNPs with producing a much smaller number of MAD particles reducing the mean diameter from 12.00 to 10.49 nm and the PDI data from 0.0220 to 0.0086 supported this fact. MNPs show a higher particle size distribution as compared to MAD with lower particle size distribution (Fig. 6b). After aggregation, the particles are distributed in the smaller area due to disruption of self-aggregated MNPs. With the SB and MTX, the MD is found at 1.13 [33] and 12.47 nm respectively. The higher value of MTX as compared to SB inferred the structural difference between them. The MD of the complex aggregation are 11.39 and 11.07 nm for SB- MAD and MTX-MAD respectively, inferred the structural changes after complex formation as compared to both alone due to encapsulation in MAD. The DLS data analysis showed PDI for TTDMM, MNPs and MAD as 0.0220, 0.1128 and 0.0086 respectively.

The PDI of MAD found at 0.0086 is lower by 0.1042 as compared to pure MNPs. The MNPs shows a higher PDI as compared TTDMM and MAD due to their milder tendency for self-aggregation via columbic forces responsible for their superparamagnetic properties [49]. The PDI for SB and MTX are found as 0.0713 and 0.0081. After their encapsulation with MAD, the PDI found at 0.02065 and 0.04630 for SB-MAD and MTX-MAD inferred effective aggregation with an involvement of HB and hydrophobic interactions (Fig. 6b).

The low PDI value indicates the uniform particle size distribution of SB-MAD as compared to MTX-MAD which may due to the structural difference for optimized through binding. It is interesting that the SB–MAD and MTX-MAD complex formation have been highly ordered and reoriented towards MNPs structure. Branches on the surface of TTDMM are responsible for the hyper-branched complex formation and moderated by the architecture of MAD. The MAD and their complexes with SB and MTX were uniform in size that showed by the MD and high PDI values, inferred the homogeneous distribution of SB and MTX without any collapsed particles in the interstices of MAD.

3.6 Morphological study

The close visual inspection of MNPs, TTDMM, MAD, SB, MTX, SB-MAD and MTX-MAD, definite differences in their morphologies were obtained (Figs. 7a-7g) that confirmed their shape, appearance and composition by SEM-EDX (Figs. 8a- 8c). The micrograph for TTDMM shows almost an equal distribution of molecular geometries with spherical and thinner threadlike structures in a form of crystalline shapes. These are branched and are distributed with almost equal sizes (Fig. 7b).

The MAD has shown almost spherical and compact structure but the pure TTDMM have shown a thicker stick-like structure with their equal distribution (Figs. 7b, 7c). The MNPs smaller sized particles are aggregated in TTDMM with a larger shaped sparingly distributed with larger surface area as seen in the MAD image (Figs. 7b, 7c). Their EDX analysis shows weight % of C (62.88), O (37.12) and atomic % of C (69.29), O (30.71) for TTDMM. The weight % found as C (53.68), O (42.38), Fe (3.96) and atomic % of C (62.18), O (36.84), Fe (0.99) for MAD (Table 1), inferred the aggregation pattern of MNPs in TTDMM. The highly branched and spherical structural morphology of MAD shows higher MD values than those of MNPs found from DLS.

The SB displayed a plate-like crystal pattern, having typically long and narrow crystal-like pine leaves and possessed a sharp point. This inferred that the benzene rings in the SB structure are unable to fold (Fig. 7d). Whereas, in the SB-MAD morphology image exhibited a well-defined spherical shaped, SB form a compact structure with MAD after encapsulation (Fig. 7e). This infers that the SB even solid form has clusters of different geometries may be due to many benzene rings with many -OH groups whose activities are monitored with their motions (Fig.1). The EDX analysis is given in table 2, in the SB weight % of C (73.02), O (26.98) and atomic % of C (78.28), O (21.72) and for SB-MAD, the weight % are C (55.11), O (34.96), Fe (8.81) and atomic % of C (65.81), O (31.34), Fe (2.26). From these results it is clearly understood that amount of SB bind with MAD is responsible for complexation. The pure MTX showed a reticulated lattice, cubic structure, consisting of small crystals (Fig. 7f). Whereas MTX-MAD exhibited a well-defined spherical shaped, forming a compact structure (Fig 7g). The SEM image of MTX-MAD revealed that the MTX with MAD was formed smooth structural aggregation.

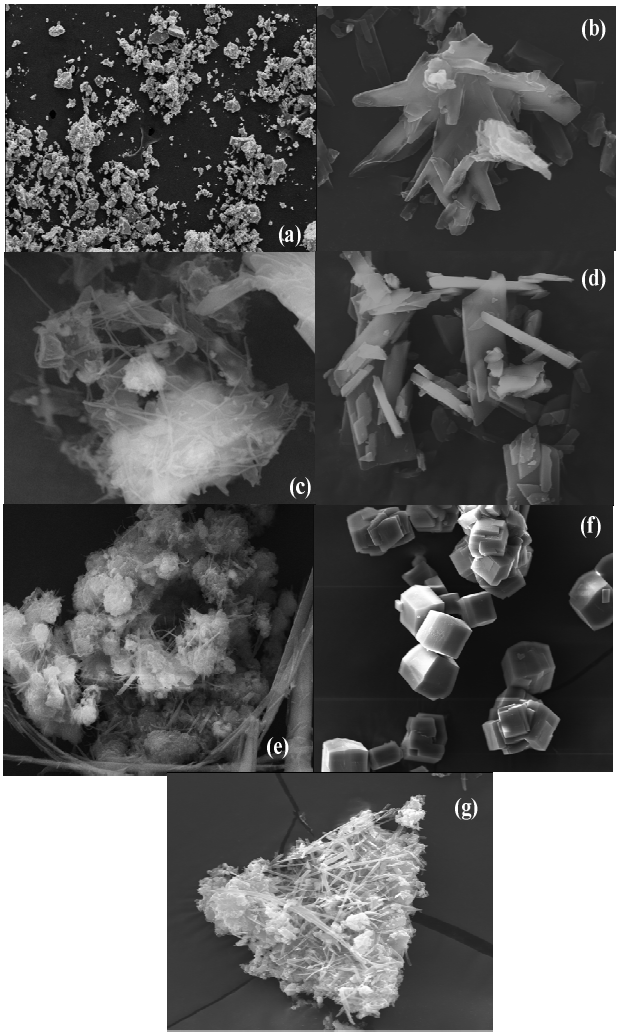

Fig.7. SEM micrograph of (a) MNPs, (b) TTDMM, (c) MAD, (d) SB, (e) SB-MAD, (f) MTX, and (g) MTX-MAD

The EDX analysis of MTX, the weight % of C (48.93), O (18.60), N (32.47) and atomic % of C (53.93), O (15.39), N (30.68) were found. In case of MTX-MAD, the weight % of C (35.56), O (29.65), N (21.21), Fe (13.58) and atomic % of C (48.07), O (27.16), N (17.75), Fe (7.02), this revealed that the MTX with MAD induced remarkable changes in the surface morphology of the MAD (Table 2). Small cubic crystals of MTX bind with MAD to a 3D network, driven by an involvement of HB, hydrophobic and electrostatic interactions. Hence, the incorporation of SB and MTX in MAD may be an effective drug delivery system. Hence, the MAD is most effective in holding the SB and MTX acting as a cap to hold during transportation. However, drug-MAD complex formation did not depend on the structural changes but, SEM-EDX can easily detect the morphological and compositional changes carried out during encapsulation process and so it can further give confirmatory data for drug interaction with MAD. Thus, the critical variations in the internal morphologies of MAD suggested that the SEM images of SB-MAD and MTX-MAD showed SB and MTX encapsulation/conjugation in their structure.

Table. 2. Elemental analysis with EDX.

Sample	Elements							
	Weight (%)				Atomic (%)			
	C	O	N	Fe	C	O	N	Fe
TTDMM	62.88	37.12	-	-	69.29	30.71	-	-
MAD	53.68	42.38	-	3.96	62.18	36.84	-	0.99
SB	73.02	26.98	-	-	78.28	21.72	-	-
MTX	48.93	18.60	32.47	-	53.93	15.39	30.68	-
SB-MAD	55.11	34.96	-	8.81	65.81	31.34	-	2.26
MTX-MAD	35.56	29.65	21.21	13.58	48.07	27.16	17.75	7.02

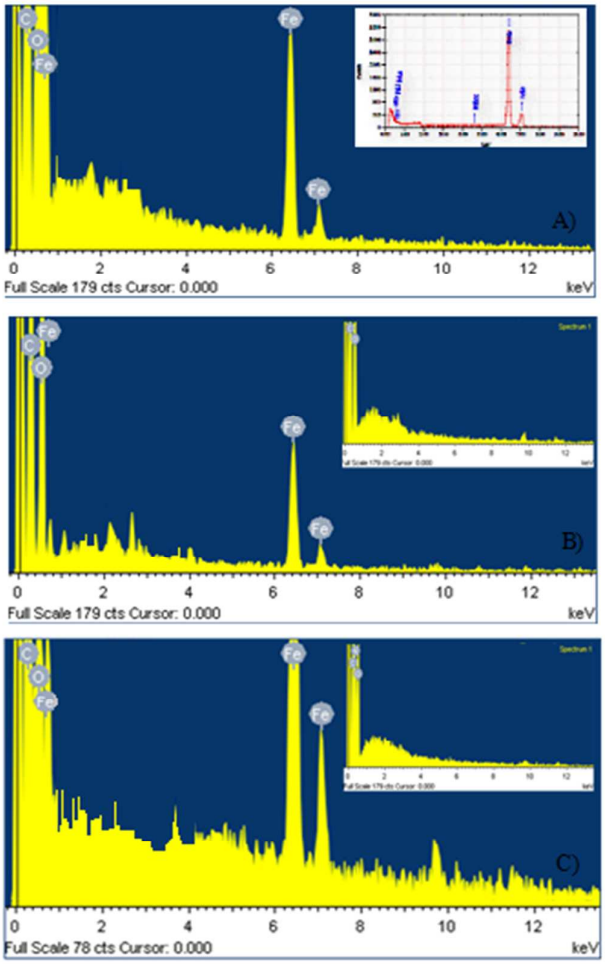

Fig. 8. EDX pattern of A) MAD, B) SB-MAD and C) MTX-MAD, inset at right shows EDX of pure MNPs, SB and MTX respectively

3.6 *In vitro* drug release from MAD

The entrapment efficiency of SB and MTX is found as 88.23%±2% and 80.37%±5% respectively. The releasing behavior of the drug from the carrier system is an important factor because the effects of the drug to cure the disease depend on the concentration. The characterization through FTIR, DLS and SEM of MAD has shown a good capacity to encapsulate SB and MTX. Encapsulation was purely based on HB and electrostatic interactions responsible for binding and releasing activities for the SB and MTX. So the releasing activities of SB and MTX from MAD as a carrier system were studied in 100 ml PD (pH 7.4, 37 °C) at 0 to 10th h predetermined time interval and the release content of SB and MTX were quantified by using UV-Vis spectroscopy.

A calibration curve of SB and MTX were obtained for 25, 50, 75, 100 and 125 µM SB (Figs. S4, S5). Also, for TTDMM at 25, 50, 75, 100 and 125 µM the UV analysis was performed (Fig. S6). For SB (at 245, 285 and 330 nm) and MTX (at λmax 260, 305 and 380 nm) in PD solution gives a maximum absorbance in the UV region at its characteristic wavelength (Figs. 9a, 9b and Table 3). At a characteristic wavelength, the absorbance increases with increasing concentration of SB and MTX. At 125 µM the absorbance values of SB at λmax 245 (1.107), 285 (1.170) and 330 (2.187) nm, and similarly for MTX at λmax 260 (1.812), 305 (1.804) and 360 (0.609) nm respectively (Figs. S4, S5 and table S1).

The complexes of SB and MTX with MAD were dissolved in the PD solution and determining the absorbance at 0-10 h predetermined time interval for drug release activities for both of them. Since the SB-MAD and MTX-MAD in the PD solutions produce absorbance at (245, 285 and 330 nm) λmax for SB and at (260, 305 and 380 nm) λmax for MTX, the absorbance obtained from solutions belong to SB and MTX respectively (Figs. 10a, 10b and table S1). These absorbance values were correlated to their calibration curves for determining the amount of SB and MTX separately. *In vitro* release of SB from MAD has observed a sustainable process with an initial release monitored by a slow release (Fig. 11a and Table S2). However, significant release of SB in the present study was slower and sustainable.

The MTX release from TTDMM (Fig. S7) and MAD shows initial burst release with a decrease in the concentration of MTX in PD Medium as no drug content was bounded with the carrier. As MTX contains the two $-NH_2$, five nitrogen atoms and two -COOH group which are responsible for the ceasing motions and molecular folding through hydrogen bonding between $-NH_2$ and –COOH groups. Such intramolecular activities of MTX developed a cubic structure, smaller sized and high density facilitating their entry in the void spaces by weakest Vander-Waals forces; it has been supported through the entropic motions of branching molecules. So, in absence of weakest binding forces the MTX quickly burst out into the medium contrary to SB. Although MAD shows more control on the release of MTX than TTDMM.

Table. 3. Absorbance values of TTDMM [33], SB and MTX concentration (µM) in PD.

µM	TTDMM*	SB λ_{max}(nm)			MTX λ_{max}(nm)		
	240 nm	245	285	330	260	305	380
25	0.508	0.242	0.224	0.518	0.349	0.36	0.116
50	0.870	0.465	0.454	1.074	0.758	0.787	0.237
75	1.182	0.682	0.678	1.606	1.151	1.179	0.365
100	1.208	0.890	0.918	1.987	1.53	1.559	0.491
125	1.236	1.107	1.170	2.187	1.812	1.804	0.609

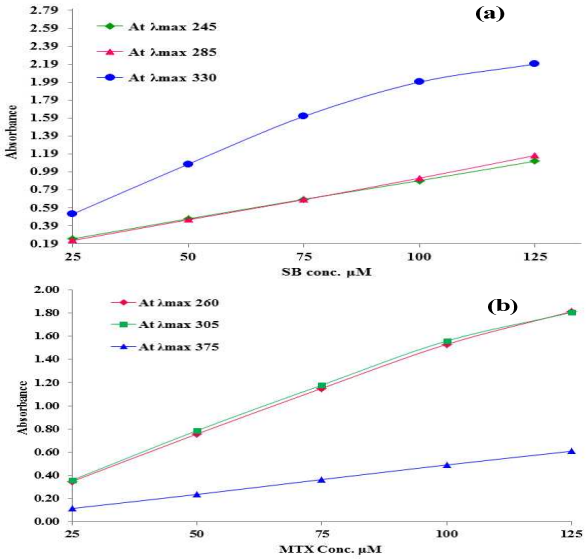

Fig.9. Standard absorbance calibration curve of SB at λmax of 245, 285, 330 nm and MTX at λmax of 260, 305, 375 nm

A release profile of SB has inferred a higher solubility in PD (pH 7.4, 37 0C) as compared to water. The SB release is increased from 0.58 to 52.51 % in 0-10 h (Fig. 11a and table S2).The Singh et al have reported the SB binding and releasing the study with 1st tier dendrimers and the release of SB strongly moderated by the interstices of dendrimers [33].

The SB has shown higher and sustainable release activity from MAD as compared to TTDMM (Fig. 11b). This has proven the impact of MNPs on controlling the releasing behavior of SB, which is 0.58 % initially (Fig. 11a and table S2) whereas with TTDMM it was 3.95% as reported. It has been inferred a development of HB and hydrophobic interactions with MAD as a major mechanism for SB binding and releasing activity. Interestingly, the role of MNPs with TTDMM dendrimer was shown to enhance an encapsulation and release behavior of SB.

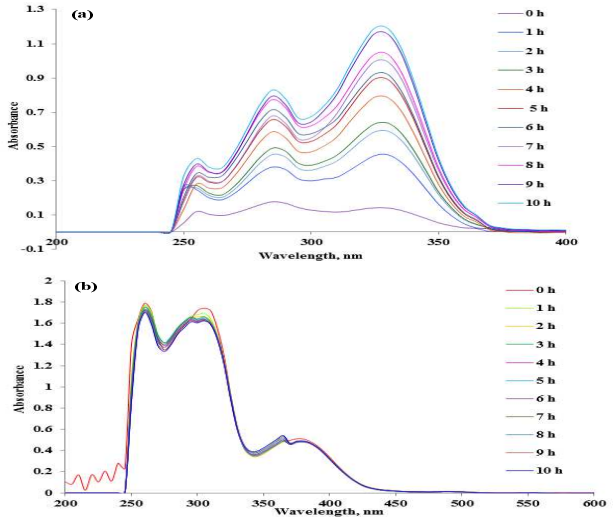

Fig.10. UV–Vis absorbance spectra of (a) SB-MAD and (b) MTX-MAD

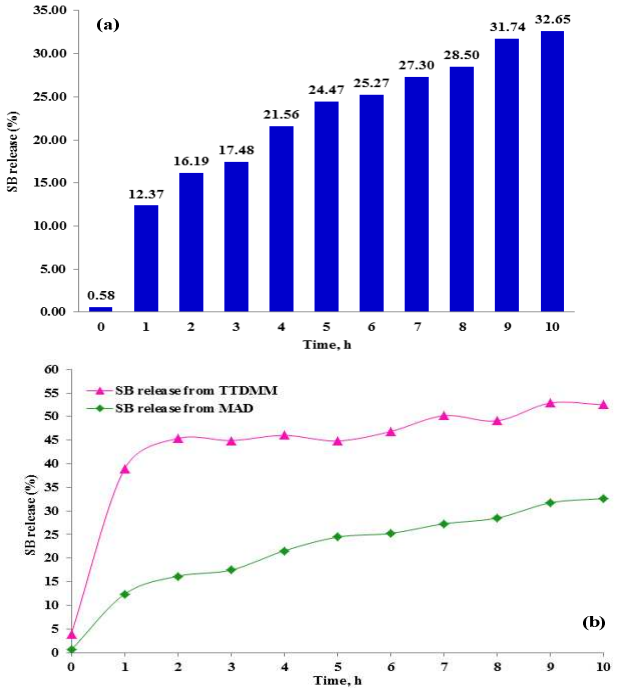

Fig.11. (a) SB release profile (%) from MAD and (b) The comparison of SB release from MAD with reported TTDMM [33]

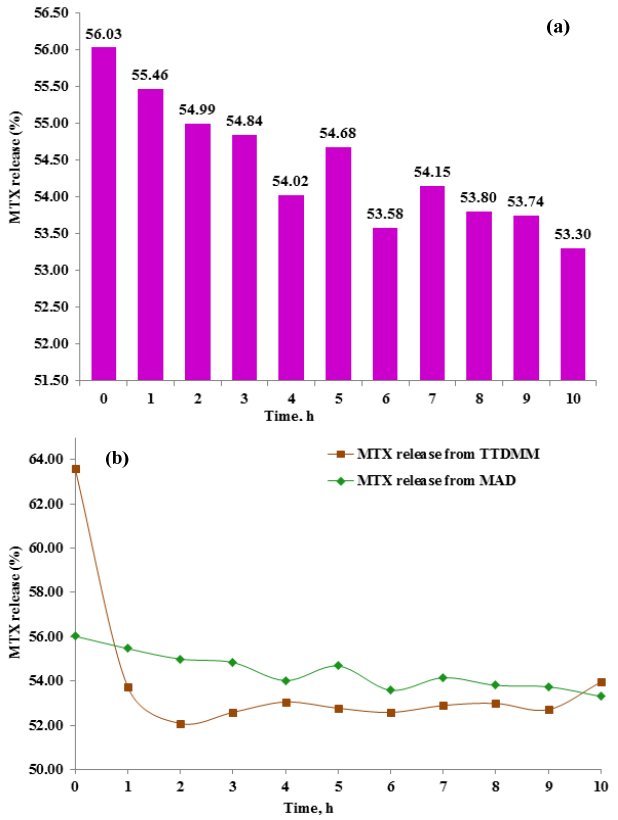

Fig.12. (a) MTX release profile (%) from MAD and (b) The comparison of MTX release from MAD with TTDMM

In case of MTX-MAD, during the initial hour ≈ 56.03 % MTX release from MAD was observed (Fig. 12a and table S2). Followed by a prolonged release (up to 10th h) with reduced the amount of MTX. The initial higher release may be probably caused by the binding of MTX on the surface of the MAD which could be disrupted by PD medium. However, similar release pattern was found with TTDMM but the difference was, the MTX shows burst release up to 63.60% which was controlled by MAD (Fig. 12b). But in case SB, the sustained release was obtained due to encapsulation of SB inside the MAD. (Figs. 11a, 11b and table S2).

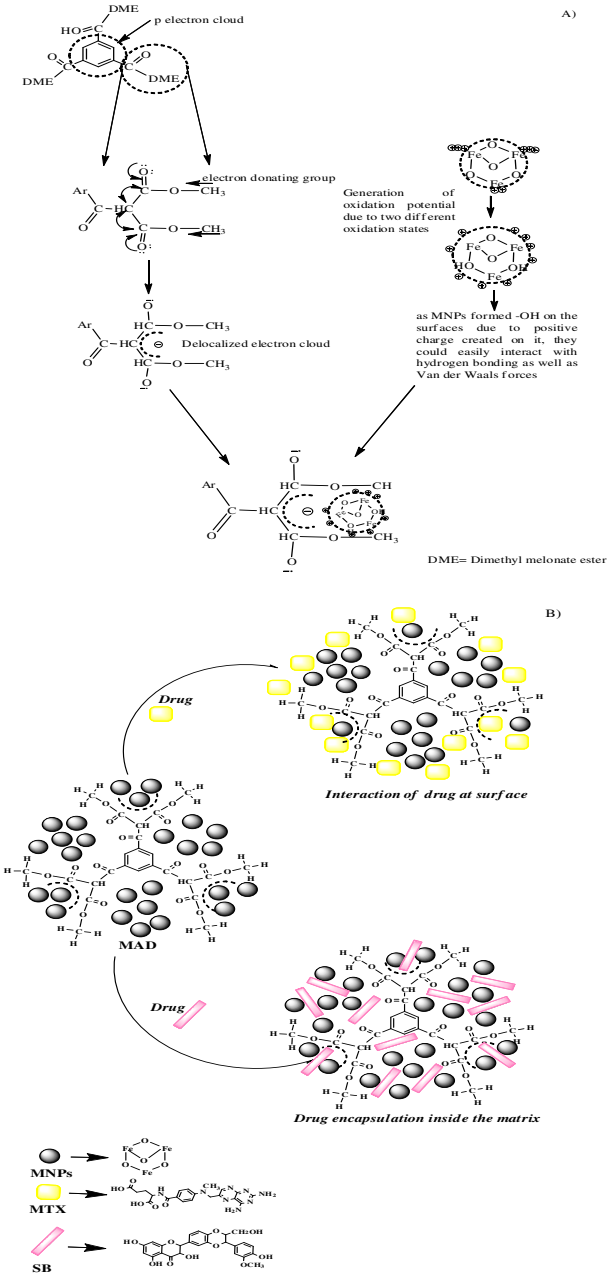

Fig.13. A) Mechanistic Model for MAD formation, and B) Pictorial model depicting conjugation and encapsulation of drug molecule with MAD

The rapid initial release may be attributed to the fraction of MTX weakly bound to the surface of MAD. This is because the mean size of MTX (12.47) is greater than of the MAD (10.49) as found in DLS. However, MAD is the complex of MNPs and 1st tier dendrimer having very less diameter, where MNPs occupied the void spaces and so MTX could not enter to that cavity resulting to surface conjugation. The in vitro drug release results revealed that the prepared SB-MAD complexes could be able to control drug release for an extended period of time. Hence, MAD provides a uniform platform for SB attachment that has the ability to bind and control the release of SB through HB and hydrophobic interacting mechanisms. In this case, the thermodynamic equilibrium plays a critical role, where drug could show higher affinity of interaction with dendrimer than MNPs and it could lead to control on the release of the drug molecules in a particular ratio. Here, the ration inferred the release rate of drug where drug may show a particular pattern as firstly it will detach from MNPs and go with dendrimer, although dendrimers having void spaces, it will lose the drug in particular amount and this will generate vacancies for another drug molecule and it will be further forwarded till total drug released from the carrier. However, MNPs could interact with both the molecules of dendrimers and drug which resulted into the sustain release of SB which is having more electronegative functional groups and delocalized electron clouds, but this environment was not found with MTX which is having a nitrogen rich environment resulting to surface adsorption on MAD.

3.7 Chemosensitivity test (SRB assay)

The SRB assay was carried out to determine the drug sensitivity with reference to increasing the concentration of the drug on human lung cancer cell line. The result shows that MNPs and MAD did not show any effect on the inhibition of cell growth, whereas SB and MTX from MAD show the significant effect. The SB shows growth inhibition at higher concentration as 40 and 80 µg/ml of total complex, this is due to sustained release of SB from MAD which is only 1.15% initially and 24.75% after 1 h incubation at 37 °C.

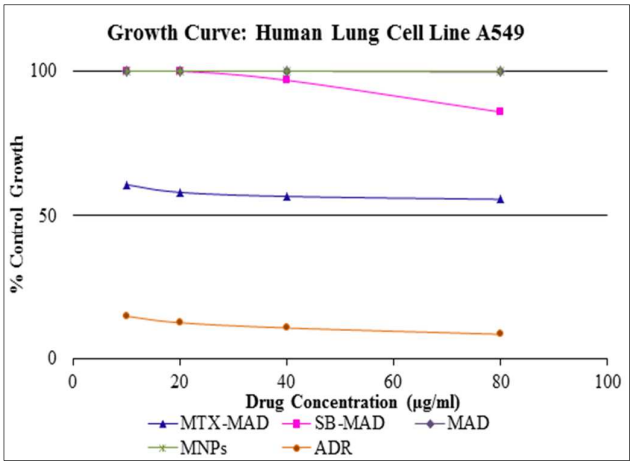

Fig.14. In vitro chemosensitivity test of 20 to 80 µg/ml SB-MAD and MTX-MAD on Human Lungs cancer cell line A549 in DMSO

Whereas, MTX shows good potential to inhibit the proliferation of A549 cells (76.2 %) with growth inhibition of 50 % (GI50), resulting from the 50 % reduction in the net protein increase (Fig. 14). This shows better absorption of MTX via cell which may due to the initial release (93.52 %) of MTX from MAD in a medium. These data support the in vitro drug release profile of SB and MTX from the MAD in PD (Figs. 11a, 12a). Hence, the SRB assay inferred that A549 cell line is more chemosensitive for MTX as compared to SB because of fewer drugs absorbed through cells, which can result in the inhibition of cell proliferation/ protein synthesis.

4. Conclusion

The MNPs accumulated TTDMM has improved their solubility in PD, in order to ensure sustainable drug release. Drug-MAD complexes with structural reorientation of SB and MTX were characterized by using FTIR, DLS and SEM inferred the MAD as a potential SB and MTX carrier. The UV-Vis analysis showed a sustained release of SB from MAD in PD attribute encapsulation of SB through MAD resulting control on the release. However, MTX release could not control through MAD as it is show burst release initially inferred weak interaction of drug via surface conjugation. This may overcome by increasing branching of dendrimer for preparing MAD, as this will result into a high surface area and large void spaces for encapsulating various drugs. Thus, reduced SB and MTX release are beneficial for controlling a release rate in drug delivery system. These significant results have suggested that HB and hydrophobic interaction have developed an intramolecular multiple forces for encapsulated of SB and MTX in MAD with major effect on its binding and release activities. This study inferred that MAD is potential SB and MTX vehicles and also it offers several attractive features for developing potential drug delivery systems.

Acknowledgments

Authors are thankful to Central University of Gujarat, Gandhinagar, for infrastructural support. Also thankful to Advance Center for Treatment, Research and Education in Cancer (ACTREC), TATA memorial centre, Mumbai for chemosensitivity test, Department of Forensic Science, Gandhinagar, Gujarat for SEM-EDX analysis and magnetization lab, UGC-DAE Consortium for Scientific Research, Indore center for VSM measurements.

References

1. R. X. B. Du. Zhuo, Z. R. Lu, J. Controlled Release, 1999, **57**, 249-257. doi: 10.1016/S0168-3659(98)00120-5
2. W. Wei, H. Quanguo, J. Changzhong, Nanoscale Res Lett., 2008, **3**, 397– 415. doi: 10.1007/s11671-008-9174-9
3. L. H. Reddy, J. L. Arias, J. Nicolas, P. Couvreur, Chem. Rev., 2012, **112**, 5818−5878. doi: 10.1021/cr300068p.
4. N. A. Frey, S. Peng, K. Cheng, S. Sun, Chem. Soc. Rev., 2009, **38**, 2532–2542. doi: 10.1039/b815548h.
5. T. Neuberger, B. Schöpf, H. Hofmann, M. Hofmann, B. Rechenberg, J. Magn. Magn. Mater., 2005, **293**, 483-496. doi: 10.1016/j.jmmm.2005.01.064.
6. D. Portet, B. Denizot, E. Rump, J. J. Lejeune, P. Jallet, J. Colloid Interface Sci., 2001, **238**, 37- 42. doi: 10.1006/jcis.2001.7500
7. A. Jordan, R. Scholz, K. Maier-hauff, M. Johannsen, P. Wust, , J. Nadobny, H. Schirra, H. Schmidt, S. Deger, S. Loening, J. Magn. Magn. Mater., 2001, **22**, 5118–1265. doi: 10.3109/02656731003745740
8. A. Senyei, K. Widder, G. Czerlinski, J. Appl. Phys., 1978, **49**, 3578-3583. doi: 10.1063/1.325219.
9. K. J. Widder, A. E. Senyei, G. D. Scarpelli, Proc. Soc. Exp. Biol. Med., 1978, **158**, 141–146. doi: 10.3181/00379727-158-40158
10. A. S. Lubbe, C. Bergemann, W. Huhnt, Cancer Res., 1996, **56**, 4694-4701. doi: http://cancerres.aacrjournals.org/content/56/20/4694
11. A. S. Lubbe, C. Bergemann, H. Riess, Cancer Res. 1996, **56**, 4686-4693. Doi:http://cancerres.aacrjournals.org/content/56/20/4686.long
12. J. Koda, A. Venook, E. Walser, S. Goodwin, Eur. J. Cancer, 2002, **38**, (Suppl 7):S18. doi: 10.1016/s0959-8049(02)80690-6
13. T. K. Jain, J. Richey, M. Strand, D. L. Leslie-Pelecky, C. A. Flask, V. Labhasetwar, Biomaterials, 2008, **29**, 4012–402. doi:10.1016/j.biomaterials.2008.07.004.
14. B. Koppolu, M. Rahimi, S. Nattama, A. Wadajkar, K.T. Nguyen, Nanomedicine, 2010, **6**, 355-361. doi:10.1016/j.nano.2009.07.008.
15. S. Purushotham, R. V. Ramanujan, Acta Biomater., 2010, **6**, 502-510. doi:10.1016/j.actbio.2009.07.004.
16. K. Katagiri, M. Nakamura, K. Koumoto, ACS Appl. Mater. Interfaces., 2010, **2**, 768-773. doi: 10.1021/am900784a.
17. C. Ravikumar, S. Kumar, R. Bandyopadhyaya, J. Colloids Surf., 2012, **A 403**, 1–6. doi: 10.1016/j.colsurfa.2012.02.007.
18. H.-W. Yang, M.–Y. Hua, H.–L. Liu, C.–Y. Huang, K.–C. Wei, Nanotech Sci and App., 2012, **5**, 73–86. doi: http://dx.doi.org/10.2147/NSA.S35506
19. A. L. Glover, J. B. Bennett, J. S. Pritchett, S. M. Nikles, D. E. Nikles, J. A. Nikles, C. S. Brazel, IEEE Trans Magn. 2013, **49**, 231–235. doi: 10.1109/TMAG.2012.2222359
20. S. Sieben, C. Bergemann, A. LuKbbe, B. Brockmann, D. Rescheleit, J. Magn. Magn. Mat. 2001, **225**, 175-179. doi: 10.1016/S0304-8853(00)01248-8.
21. C. Wilhelma, C. Billoteya, J. Roger, J. N. Pons, J.-C. Bacria, F. Gazeaua, Biomaterials, 2003, **24**, 1001–1011. doi: 10.1016/S0142-9612(02)00440-4
22. J. W. Lee, B. K. Kim, H. J. Kim, S. C. Han, W. S. Shin, S. H. Jin, Macromolecules, 2006, **39**, 2418–2422. Doi: 10.1021/ma052526f
23. S. Hong, P. R. Leroueil, E. K. Janus, J. L. Peters, M.M. Kober, M.T. Islam, B.G. Orr, J. R. Jr. Baker, M.M. Banaszak Holl, Bio conjugate Chem. 2006, **17**, 728–734. doi: 10.1021/bc060077y
24. S. Svenson, D. A. Tomalia, Adv. Drug. Deliv. Rev., 2005, **57**, 2126–2129. doi:10.1016/j.addr.2005.09.018
25. X. Q. Li, D. W. Elliott, Wei-x. Zhang, T&F Critical Rev. in solid state and Mater., 2006, **31**, 111-122.DOI: 10.1080/10408430601057611
26. R. P. Patel, Pharma Bio World., 2007, 42-52.
27. B. Pan, D. Cui, Y. Sheng, C. Ozkan, F. Gao, R. He, Cancer Res., 2007, **67**, 8156–8163. doi: 10.1158/0008-5472.CAN-06-4762
28. Y. Chang, X. Meng, Y. Zhao, K. Li, B. Zhao, M. Zhu, Y. Li, X. Chen, J. Wang, J. Colloid Interface Sci. 2011, **363(1)**, 403-409. doi: 10.1016/j.jcis.2011.06.086.
29. K. Rouhollah, M. Pelin, Y. Serap, U. Gozde, G. Ufuk, J. Pharm. Sci., 2013, **102**, 1825-1835. doi: 10.1002/jps.23524
30. R. Khodadust, G. Unsoy, U. Gunduz, Biomed Pharmacotherapy, 2014, **68(8)**, 979-987. doi: 10.1016/j.biopha.2014.10.009.
31. B. F. Pan, F. Gao, H. C. Gu, J. colloid Interface sci. 2005, **284**, 1-6. doi:10.1016/j.jcis.2004.09.073
32. S. Dietrich, 2011. Technische Universität Chemnitz, Fakultätfür Naturwissenschaften, Dissertation, **165** Seiten. doi: urn:nbn:de:bsz:ch1-qucosa-82016
33. S. B. Undre, M. Singh, R. K. Kale, Md. Rizwan, J. Appl. Polym. Sci., 2013, **130**, 3537-3554. doi: 10.1002/app.39466
34. S. R. Pandya, M. Singh, J. Mol. Liq., 2015, **211**, 146-156. Doi: http://dx.doi.org/10.1016/j.molliq.2015.06.068
35. P. Morazzoni, E. Bombardelli, Fitoterapia., 1995, **66**, 3-42.
36. V. G. Hahn, H. D. Lehmann, M. Kurten, H. Uebel, G. Vogel, Arzneimittelforsch., 1969, **18**, 698-704.
37. B. N. Cronstein, J. R. Bertino, Milestones in Drug Therapy-Methotrexate, Birkhäuser Verlag, A.G. (Eds.), Basel-Berlin-Boston, Switzerland, 2000, 252 p. Doi: 10.1023/a:1016127228198
38. P. Morazzoni, A. Montalbetti, S. Malandrino, G. Pifferi, Eur. J. Drug Metab. Pharmacokinet., 1993, **18**, 289-297. doi: 10.1007/BF03188811
39. S. Luper, Alt. Med. Rev. 1998, **3**, 410-421. Doi: http://www.altmedrev.com/publications/3/6/410
40. J. Pepping, Am. J. Health Syst. Pharm. 1999, **56**, 1195-1197.

41. J. Sun, S. Zhou, P. Hou, Y. Yang, J. Weng, X. Li, M. Li. J. Biomed. Mat. Res., 2006, **80A,** 333-341. Doi: 10.1002/jbm.a.30909
42. Y. Hu, X. Jiang, Y. Ding, L. Zhang, C. Yang, J. Zhang, J. Chen, Y Yang,, Biomaterials, 2003, **24**, 2395- 2404. doi:10.1016/S0142-9612(03)00021-8
43. E. K. Park, S. B. Lee, Y. M. Lee, Biomaterials, 2005, **26(9)**, 1053-1061.Doi:10.1016/j.biomaterials.2004.04.008
44. Y. Ling, Y. S. Huang, 7th Asian-Pacific Conference on Medical and Biological Engineering (APCMBE), IFMBE Proceedings. Peng, Y., Wen, X., (Eds). Springer, Berlin, Heidelberg, 2008, **19**, 514–517. doi : 10.1007/978-3-540-79039-6_129
45. R. S. Kalkotwar, A. V. Kasture, S. R. Pattan, S. S. Dengale, , N. S. Dighe Der. Pharma. chemica. 2010, **2**, 127-133. Doi: http://derpharmachemica.com/vol2-iss1/DPC-2010-2-1-127-133
46. H. Unterweger, R. Tietze, C. Janko, J. Zaloga, S. Lyer, S. Dürr, N. Taccardi, O. M. Goudouri, A. Hoppe, D. Eberbeck, D. W. Schubert, A. R. Boccaccini, C. Alexiou, Int. J. Nanomedicine., 2014, **9,** 3659–3676. DOI http://dx.doi.org/10.2147/IJN.S63433
47. K. Landfester, L. P. Ramirez, J. Phy. Condense. Matter, 2003, **15**, s1345-s1362.
48. F. Zaeraa, Chem. Soc. Rev., 2014, **43**, 7624–7663. DOI: 10.1039/c3cs60374a
49. R. P. Tan, J. Carrey, C. Desvaux, J. Grisolia, P. Renaud, B. Chaudret, M. Respaud, Phys. Rev. Lett., 2007, **99**, 176805(4). doi: 10.1103/PhysRevLett.99.176805

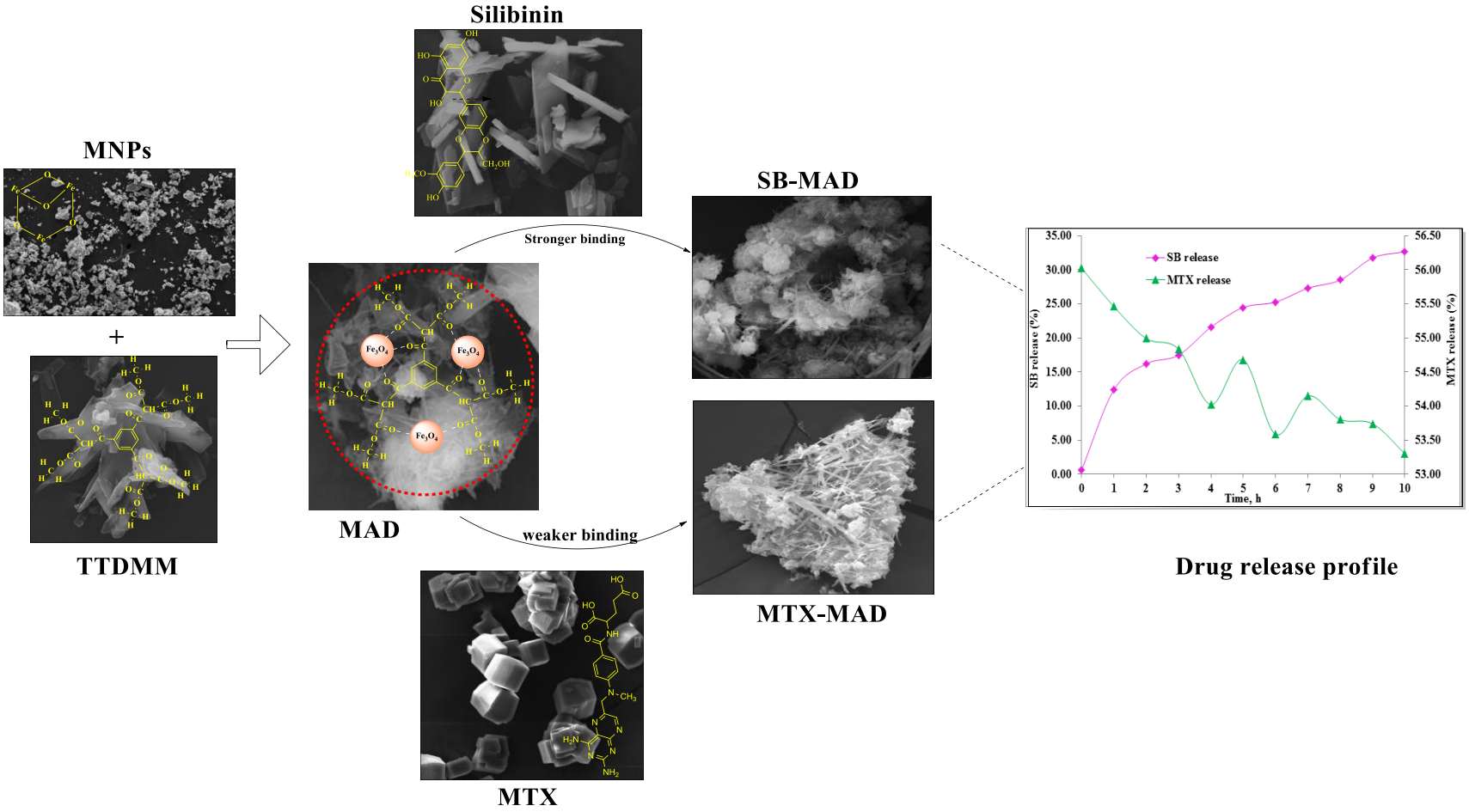

Figure depicts the morphological changes of MAD to Drug-MAD complex and that complex used for SB and MTX release study from MAD, occurred in phosphate buffer saline with 10% DMSO, with time in h. The absorbance is plotted as function of wavelength at 245, 285 and 330 nm for SB and 260, 305 and 375 nm for MTX and found that SB shows sustained release whereas MTX shows burst release from MAD.